# Optical particle sorting on an optofluidic chip

**Kaelyn D. Leake,[1,*] Brian S. Phillips,[2] Thomas D. Yuzvinsky,[1] Aaron R. Hawkins,[2] and Holger Schmidt[1]**

[1] *School of Engineering, University of California Santa Cruz, 1156 High Street, Santa Cruz, California 95064, USA*
[2] *Electrical and Computer Engineering Department, Brigham Young University, Provo, UT 84602 USA*
[*] *kaelyn@soe.ucsc.edu*

**Abstract:** We report size-based sorting of micro- and sub-micron particles using optical forces on a planar optofluidic chip. Two different combinations of fluid flow and optical beam directions in liquid-core waveguides are demonstrated. These methods allow for tunability of size selection and sorting with efficiencies as high as 100%. Very good agreement between experimental results and calculated particle trajectories in the presence of flow and optical forces is found.



**OCIS codes:** (130.3120) Integrated optics devices; (230.7390) Waveguides, planar; (350.4855) Optical tweezers or optical manipulation.

## References and links

1. R. W. Applegate, Jr., J. Squier, T. Vestad, J. Oakey, D. W. M. Marr, P. Bado, M. A. Dugan, and A. A. Said, "Microfluidic sorting system based on optical waveguide integration and diode laser bar trapping," Lab Chip **6**(3), 422–426 (2006).
2. J. Glückstad, "Microfluidics: Sorting particles with light," Nat. Mater. **3**(1), 9–10 (2004).
3. M. P. MacDonald, G. C. Spalding, and K. Dholakia, "Microfluidic sorting in an optical lattice," Nature **426**(6965), 421–424 (2003).
4. C. Liu, T. Stakenborg, S. Peeters, and L. Lagae, "Cell manipulation with magnetic particles toward microfluidic cytometry," J. Appl. Phys. **105**(10), 102014 (2009).
5. N. Pamme and C. Wilhelm, "Continuous sorting of magnetic cells via on-chip free-flow magnetophoresis," Lab Chip **6**(8), 974–980 (2006).
6. J. G. Kralj, M. T. W. Lis, M. A. Schmidt, and K. F. Jensen, "Continuous Dielectrophoretic Size-Based Particle Sorting," Anal. Chem. **78**(14), 5019–5025 (2006).
7. R. Johann and P. Renaud, "A simple mechanism for reliable particle sorting in a microdevice with combined electroosmotic and pressure-driven flow," Electrophoresis **25**(21-22), 3720–3729 (2004).
8. T. Laurell, F. Petersson, and A. Nilsson, "Chip integrated strategies for acoustic separation and manipulation of cells and particles," Chem. Soc. Rev. **36**(3), 492–506 (2007).
9. F. Petersson, L. Åberg, A.-M. Swärd-Nilsson, and T. Laurell, "Free Flow Acoustophoresis: Microfluidic-Based Mode of Particle and Cell Separation," Anal. Chem. **79**(14), 5117–5123 (2007).
10. L. Bogunovic, R. Eichhorn, J. Regtmeier, D. Anselmetti, and P. Reimann, "Particle sorting by a structured microfluidic ratchet device with tunable selectivity: theory and experiment," Soft Matter **8**(14), 3900–3907 (2012).
11. S. M. McFaul, B. K. Lin, and H. Ma, "Cell separation based on size and deformability using microfluidic funnel ratchets," Lab Chip **12**(13), 2369–2376 (2012).
12. D. Huh, J. H. Bahng, Y. Ling, H.-H. Wei, O. D. Kripfgans, J. B. Fowlkes, J. B. Grotberg, and S. Takayama, "Gravity-Driven Microfluidic Particle Sorting Device with Hydrodynamic Separation Amplification," Anal. Chem. **79**(4), 1369–1376 (2007).
13. D. Huh, W. Gu, Y. Kamotani, J. B. Grotberg, and S. Takayama, "Microfluidics for flow cytometric analysis of cells and particles," Physiol. Meas. **26**(3), R73–R98 (2005).
14. H. Cai and A. W. Poon, "Optical manipulation and transport of microparticles on silicon nitride microring-resonator-based add-drop devices," Opt. Lett. **35**(17), 2855–2857 (2010).
15. A. H. J. Yang and D. Erickson, "Optofluidic ring resonator switch for optical particle transport," Lab Chip **10**(6), 769–774 (2010).
16. S. Lin, E. Schonbrun, and K. Crozier, "Optical Manipulation with Planar Silicon Microring Resonators," Nano Lett. **10**(7), 2408–2411 (2010).
17. H. Schmidt and A. R. Hawkins, "Optofluidic waveguides: I. Concepts and implementations," Microfluid Nanofluidics **4**(1-2), 3–16 (2008).
18. R. Bernini, S. Campopiano, and L. Zeni, "Silicon micromachined hollow optical waveguides for sensing applications," IEEE J. Sel. Top. Quantum Electron. **8**(1), 106–110 (2002).

#201006 - $15.00 USD Received 8 Nov 2013; revised 6 Dec 2013; accepted 7 Dec 2013; published 23 Dec 2013

19. S. Kühn, P. Measor, E. J. Lunt, B. S. Phillips, D. W. Deamer, A. R. Hawkins, and H. Schmidt, "Loss-based optical trap for on-chip particle analysis," Lab Chip **9**(15), 2212–2216 (2009).
20. P. Measor, S. Kühn, E. J. Lunt, B. S. Phillips, A. R. Hawkins, and H. Schmidt, "Hollow-core waveguide characterization by optically induced particle transport," Opt. Lett. **33**(7), 672–674 (2008).
21. S. Kühn, E. J. Lunt, B. S. Phillips, A. R. Hawkins, and H. Schmidt, "Optofluidic particle concentration by a long-range dual-beam trap," Opt. Lett. **34**(15), 2306–2308 (2009).
22. A. Ashkin, "Forces of a single-beam gradient laser trap on a dielectric sphere in the ray optics regime," Biophys. J. **61**(2), 569–582 (1992).
23. K. D. Leake, A. R. Hawkins, and H. Schmidt, "All-optical particle trap using orthogonally intersecting beams," Photonics Res. **1**(1), 47–51 (2013).
24. S. B. Kim and S. S. Kim, "Radiation forces on spheres in loosely focused Gaussian beam: ray-optics regime," J. Opt. Soc. Am. B **23**(5), 897–903 (2006).

## 1. Introduction

Frequently, biological applications require the separation of particles within a mixture. The ability to do this sorting on chip is ideal since it requires less handling of the sample and allows for smaller sample sizes. Previously reported sorting schemes involve optical [1–3], magnetic [4,5], electrical [6,7], acoustic [8,9] or mechanical [10–12] methods of separating objects by size or index, with sorting efficiencies ranging from 75% to 100%. Some of these options require an aspect of detection before separation [4,13], adding unwanted complexity. Recently, optofluidic sorting based on microparticle manipulation by evanescent fields was demonstrated by using optical gradient forces to draw particles from a fluidic channel onto a microring resonator [14–16]. Deliberate sorting based on specific particle properties, however, has not yet been demonstrated.

Here, we introduce an optofluidic approach to on-chip particle sorting in which optical forces are used to selectively remove particles from a fluidic channel based on their size. The particles experience the full intensity of a confined liquid-core waveguide mode, keeping the required power low. Using different arrangements of optical beam and pressure-based flow directions, we demonstrate two particle removal schemes that offer tunable control over both the minimum particle size to be removed from the mixture and the removal efficiency (up to 100%). The particle removal process is automatic in that the selectivity is defined by the optical beam properties and no additional detection step is required to make a decision.

## 2. Principle and methods

We employ an optofluidic platform based on liquid-core antiresonant reflecting optical waveguides (LC-ARROWs) [17,18], hollow microchannels surrounded by multiple dielectric layers that confine light inside the channel for low-loss propagation over chip-scale distances. These LC-ARROWs can be combined with solid-core ARROWs that provide an interface between external optical fiber and the microfluidic channel for a fully planar optical layout. The majority of previous work on ARROW chips has been performed on simple single liquid core channels [19], with demonstrations of various forms of optical particle manipulation, including novel optical traps [19–21]. Here, we introduce a new design, shown in Fig. 1(a) and Fig. 1(b), which uses a more extended network of liquid-core waveguides, in this case in the shape of the letter "H". Four reservoirs are epoxied over the channel ends, allowing for independent introduction of particles and pressure-based flow in various directions. The two T-intersections enable particle sorting by diverting a single particle stream into two different directions.

The underlying physical mechanism for particle removal in both configurations discussed below is the different size dependence of the forces acting upon the particles. The drag force due to the pressure-based flow obeys Stokes' law and is given by

$$F_{FLOW} = 6\pi\mu r v. \quad (1)$$

#201006 - $15.00 USD Received 8 Nov 2013; revised 6 Dec 2013; accepted 7 Dec 2013; published 23 Dec 2013

Where $\mu$ is the dynamic viscosity of the fluid, $r$ is the radius of the particle, and $v$ is the flow speed. The optical scattering force exerted by the laser beam for particles smaller than width of the waveguide mode, on the other hand, is given by

$$F_{LASER} = Q\pi \frac{nr^2}{c} I, \tag{2}$$

where $Q$ is a dimensionless factor for the efficiency of momentum transfer, $c$ is the vacuum speed of light, and $n$ is the refractive index of the fluid, and $I$ is the intensity of the light [22,23]. Since $F_{LASER}$ scales quadratically with particle size while $F_{FLOW}$ only scales linearly, we can adjust flow and laser parameters to allow smaller particles to follow the direction of flow while larger particles follow the direction of the laser beam.

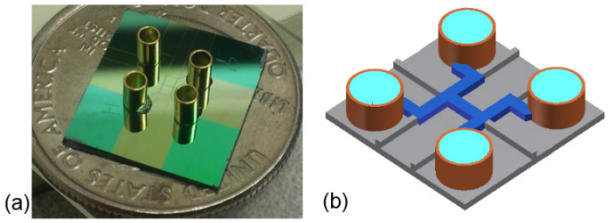


Fig. 1. (a) Image and (b) sketch of the "H" sample layout (gray: solid-core waveguides; blue: fluidic channels and liquid-core waveguides).

For a more quantitative analysis, dynamic simulations of the particle trajectories were performed. Position-dependent optical forces were calculated using formulas for loosely focused and collimated beams with the mode profiles of the LC-ARROWs [23,24]. The forces were numerically integrated to find specific values. The position-dependent drag force was calculated by using v(x,y,z) obtained from 3D simulations in COMSOL in Eq. (1). The instantaneous particle velocity was then found from the vector sum of the forces. Brownian motion was ignored since the diffusive motion of the particle was insignificant over the area of interest. This holds true for all particle sizes down to the limit (r~125nm) given by the maximum power we can supply at the intersection given our experimental parameters. By using a time step of 1ms, calculated velocities were used to advance the particle. Particle trajectories were then calculated and compared to the experimentally observed paths, which were determined by taking video screen shots and then tracking the movement of the particles through the channel. Particle sizes were determined by measuring their cross sectional area in video screen shots. Laser powers were measured at the input facet and loss values were used to calculate the powers at the T-intersection.

The experiments discussed below employed LC-ARROW chips with 5x12μm cross section and cladding layers of alternating silicon oxide and silicon nitride of thickness 3196/12/300/142/285/127nm above the liquid core and 270/93/270/93/270/93/270/93nm below the core. Laser light at 532nm (Sprout; Lighthouse Photonics) was coupled into the solid-core waveguides using single-mode fiber. The source reservoir for each layout was filled with a mixture of sulfate latex beads (r = 0.25μm, 0.5μm, 1μm and 1.5μm; Invitrogen) in a water-based solution, containing 0.05% Tween 20, 1mM sodium azide, and 8% w/v beads (with equal concentrations of each size). Well-defined and stable flows between reservoirs are created by either pumping using a Harvard Apparatus Pump or by applying hydrostatic pressure differences between the reservoirs. Both of the configurations described below were able to process up to 100 particles/second, depending on flow speed.

## 2. Results and discussion

Particle trajectories within the channel were monitored under various combinations of flow and optical laser power and analyzed to measure efficiency of optical selection and removal

#201006 - $15.00 USD Received 8 Nov 2013; revised 6 Dec 2013; accepted 7 Dec 2013; published 23 Dec 2013

of different groups of particles. There are two components of the optical force: scattering, which acts in the direction of propagation, and the gradient force, which pulls the bead into the area of greatest intensity. While the scattering force is responsible for the removal of particles, both components act together in determining the bead trajectory. The relative strengths of the forces depend on both the size of the bead and the location of the bead in the channel.

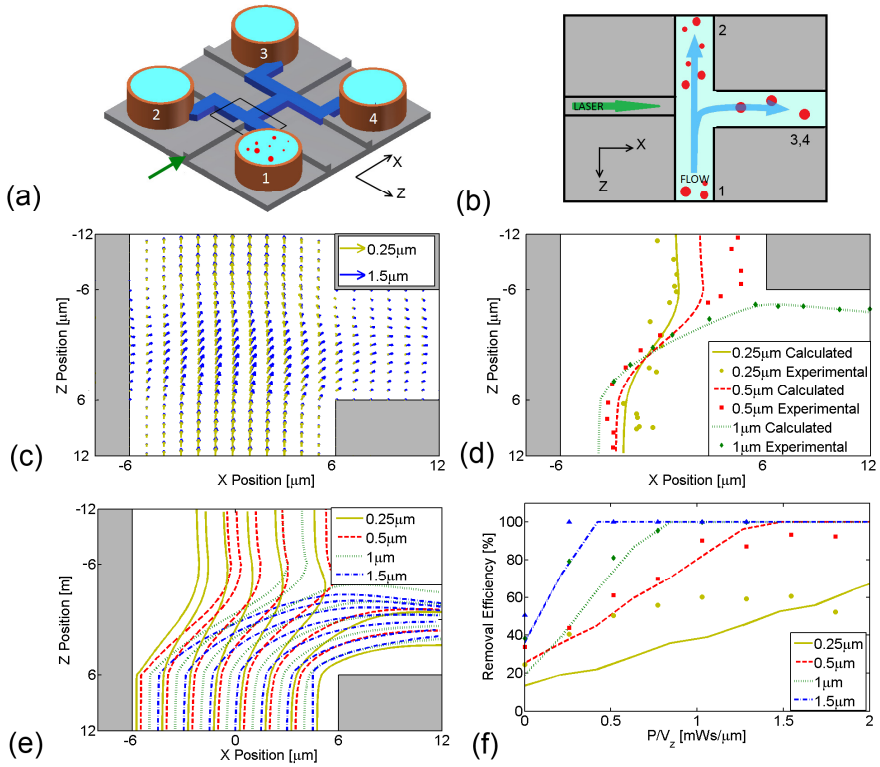


Fig. 2. The orthogonal orientation (0.25μm is gold, 0.5μm is red, 1μm is green and 1.5μm is blue). See Media 1 and Media 2 for videos in this orientation. (a) Chip layout. (b) Orientation of Laser and Flows. (c) Flow and Laser are combined to create a velocity field. (d) Flow trajectories of beads in channel (points are experimental and lines are calculated). (e) Calculated trajectories of beads in an array of starting locations with $v_z$ = 10 μm/s, $v_x$ = 0 μm/s and P = 20.1mW for the counterpropagating orientation. For the 0.25μm, 0.5μm, 1μm, and 1.5μm beads, 32%, 44%, 76% and 100% are sorted, respectively. (f) Particle removal efficiencies with $v_z/v_x$ = 0.3 (points are experimental and lines are calculated.

The first ("orthogonal") layout (see Fig. 2(a) and Fig. 2(b)) presents a pressure-driven flow of a mixture of particles with different sizes originating from reservoir 1. The flow from reservoir 1 to reservoirs 3 and 4 was minimized. At the T-intersection, the particles are exposed to a laser beam entering the channel from a solid-core waveguide perpendicular to the bulk flow. In this case, the larger particles are removed from the flow path and pushed into reservoirs 3 and 4, while the smaller particles continue flowing towards reservoir 2. The combined effect of the fluidic and the laser forces can be seen in Fig. 2(c), where the velocity vectors for the 0.25μm beads (gold) and 1.5μm beads (blue) take different paths, with the larger particles diverted into the horizontal channel. The actual motion of particles in the channel was observed and recorded (see Media 1 for the original video and Media 2 for a contrast-enhanced version). Figure 2(d) shows sample trajectories of single beads with different size; in this case the 0.25μm (gold) and 0.5μm (red) particles continue in the direction of flow whereas the 1μm (green) particles are removed. The experimental results are

#201006 - $15.00 USD Received 8 Nov 2013; revised 6 Dec 2013; accepted 7 Dec 2013; published 23 Dec 2013

shown as points and calculated trajectory is shown as the corresponding line, demonstrating excellent agreement with the data. For the coordinate system defined Fig. 2(d), particles are considered removed if $x(z=-6\mu m)>6\mu m$ .

Due to the variations of flow speed and the optical mode intensity across the channel, the lateral position of a particle as it approaches the T-intersection affects its final location. Particles approaching the intersection with x≈6μm are sorted almost instantly regardless of the size of the power, whereas particles of the same size with x≈-6μm need to move a lot farther along x and therefore may not get sorted. As seen in Fig. 2(e) this effect applies for all bead sizes, but is more significant for the 0.25μm beads due to the smaller effect of the optical force.

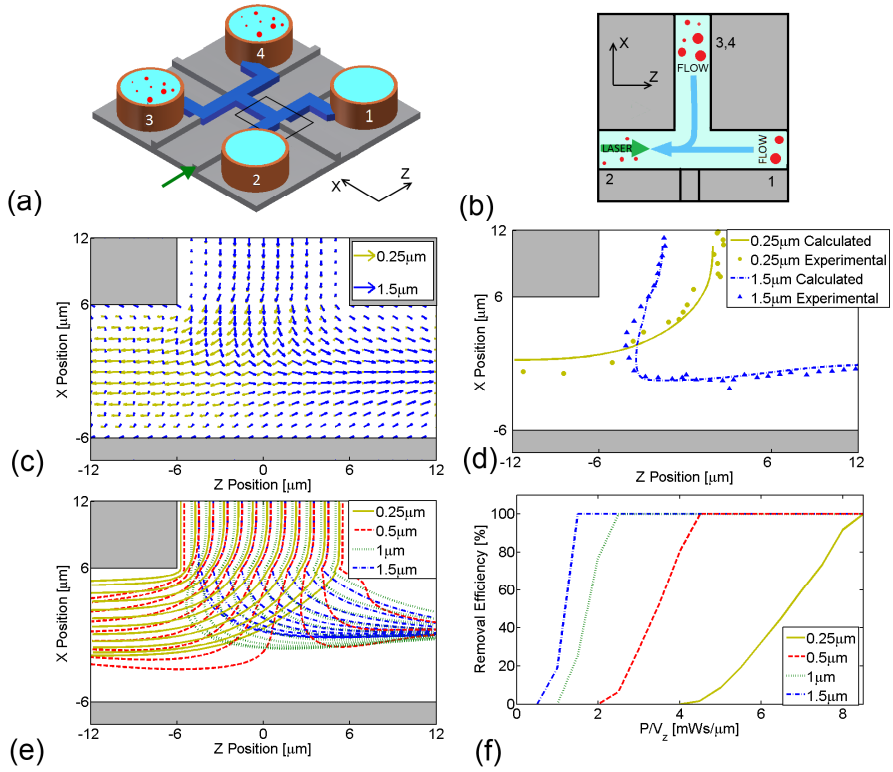


Fig. 3. The counterpropagating orientation (0.25μm is gold, 0.5μm is red, 1μm is green and 1.5μm is blue). See Media 3 and Media 4 for videos in this orientation. (a) Chip layout. (b) Orientation of Laser and Flows. (c) Flow and Laser are combined to create a velocity field. (d) Flow trajectories of beads in channel (points are experimental and lines are calculated). (e) Calculated trajectories of beads in an array of starting locations with $v_z = v_x = 10$ μm/s and P = 25mW for the counterpropagating orientation. For the 0.25μm, 0.5μm, 1μm, and 1.5μm beads, 0%, 25%, 100% and 100% are sorted respectively. (f) Calculated particle removal efficiencies with $v_z/v_x = 0.7$.

By comparing the number of beads that are removed from the flow to the total number of particles of that size, we calculate particle removal efficiency. By systematically varying the experimental conditions (flow speed, laser power), the comprehensive removal efficiency plot shown in Fig. 2(f) was created. Because the particle sorting effect is due to the difference in flow velocity compared to the velocity created by the laser, it is the relative ratio of flow velocity to power that characterizes a given parameter set. In addition, non-zero fluid flow into the horizontal channel (denoted by $v_x>0$) increases particle removal efficiency by directly

#201006 - $15.00 USD Received 8 Nov 2013; revised 6 Dec 2013; accepted 7 Dec 2013; published 23 Dec 2013

removing particles from the vertical channel. The strength of this effect increases with the ratio of $v_x$ to the vertical input flow $v_z$.

Figure 2(f) shows particle removal efficiency with $v_x/v_z$ = 0.3. Qualitatively good agreement between experiment and theory is found. The theory lines are not perfectly smooth due to the finite number of particles and lateral positions that were simulated. At low laser power, a finite and nearly size-independent removal probability is observed due to the presence of finite flow along the x-direction. As the laser power is increased, the removal efficiency can be tuned smoothly for each particle size, leading to full removal of progressively smaller particles. However, there will always be a finite fraction of smaller particles that is removed. Therefore, this geometry is best suited for tuning particle concentrations in mixtures where the complete removal of one species is not desired.

In the second ("counterpropagating") layout (see Fig. 3(a) and 3(b)), the chip is rotated to allow laser propagation along the liquid channel between reservoirs 1 and 2, with input flow adjusted to move beads from reservoir 3 (and/or reservoir 4) towards reservoir 2. In addition, a flow in the negative z-direction is introduced from reservoir 1 to reservoir 2. The laser force then acts to push larger beads along z towards reservoir 1, while smaller particles follow the flow and proceed to reservoir 2. See Media 3 for a video of this orientation in action (Media 4 shows the same video with contrast enhancement to make the beads easier to see). Particle trapping is also possible with this layout.

Depending on the relative values of both flow velocities and the power of the laser, beads at different locations will move in different directions (see Fig. 3(c)). Actual and calculated trajectories are compared in Fig. 3(d) where the 0.25μm (gold) beads continue in the direction of the flow whereas the 1.5μm (blue) beads are sorted. The criterion for sorting in this case is if a particle reaches $z = 6\mu m$. While the process is governed by the same physical principles as the orthogonal orientation, the effect of initial lateral position in the channel on particle removal is significantly weaker for the counterpropagating orientation since particles continue to feel the effects of the laser as they proceed along the negative z-direction (see Fig. 3(e)). In contrast to the orthogonal orientation, no particles are removed without optical power due to the different flow geometry (see Fig. 3(f)). Again, we find an increasing removal efficiency with optical power for each particle size. However, in this geometry it is possible to completely remove all particles above a selectable size out of a mixture while not removing any of the smaller sizes. Therefore, this geometry is best suited for selectively sorting a set of particle sizes from a stream. If combined with a second T-intersection, a "notch filter" could be created that selects only particles within a narrow size range.

## 3. Conclusion

We have introduced a method of combining pressure-based flow and optical forces in liquid-core waveguides to implement particle sorting on an optical chip. The particle removal process is automatic inasmuch as it does not require any feedback. We have demonstrated two implementations of this scheme on a single chip; one being ideal for adjusting relative particle concentrations, and one suited for eliminating all particles above a certain size from the stream. The relative concentrations and cutoff sizes can be tuned using laser power and/or flow speed. While we have focused on identical particles of different size in this work, this scheme could also be applied to select particles based on their refractive index or due to differences in shape. The simplicity of the schemes and the planar nature of the optofluidic chip suggest that this technique can be used for up-stream sample processing of liquid analytes for subsequent optical sensing and analysis on a single chip.

## Acknowledgments

We would like to acknowledge the early efforts of J. McDowell on the simulations used in this research. This work was supported by NIH/NIBIB under grant 1R21EB008802, and the W. M. Keck Center for Nanoscale Optofluidics at UCSC.

#201006 - $15.00 USD Received 8 Nov 2013; revised 6 Dec 2013; accepted 7 Dec 2013; published 23 Dec 2013